




A mutation in *DOK7* in congenital myasthenic syndrome forms aggresome in cultured cells, and reduces *DOK7* expression and MuSK phosphorylation in patient-derived iPSC cells

Shaochuan Zhang¹ , Bisei Ohkawara¹, Mikako Ito¹, Zhizhou Huang¹, Fei Zhao¹, Tomohiko Nakata¹, Tomoya Takeuchi¹, Hidetoshi Sakurai², Hirofumi Komaki³, Masayoshi Kamon⁴, Toshiyuki Araki⁴  and Kinji Ohno^{1,*} 

¹Division of Neurogenetics, Center for Neurological Diseases and Cancer, Nagoya University Graduate School of Medicine, Nagoya 466-8550, Japan

²Center for iPSC Cell Research and Application (CiRA), Kyoto University, Kyoto 606-8507, Japan

³Department of Pediatrics, National Institute of Neuroscience, National Center of Neurology and Psychiatry, Kodaira, Tokyo 187-8551, Japan

⁴Department of Peripheral Nervous System Research, National Institute of Neuroscience, National Center of Neurology and Psychiatry, Kodaira, Tokyo 187-8551, Japan

*To whom correspondence should be addressed at: Division of Neurogenetics, Center for Neurological Diseases and Cancer, Nagoya University Graduate School of Medicine, 65 Tsurumai, Showa-ku, Nagoya 466-8550, Japan. Tel: +81 52 744 2446; Fax: +81 52 744 2449; Email: ohnok@med.nagoya-u.ac.jp

Abstract

At the neuromuscular junction, the downstream of tyrosine kinase 7 (*DOK7*) enhances the phosphorylation of muscle-specific kinase (MuSK) and induces clustering of acetylcholine receptors (AChRs). We identified a patient with congenital myasthenic syndrome (CMS) with two heteroallelic mutations in *DOK7*, c.653-1G>C in intron 5 and c.190G>A predicting p.G64R in the pleckstrin homology domain. iPSC cells established from the patient (CMS-iPSCs) showed that c.653-1G>C caused in-frame skipping of exon 6 (120 bp) and frame-shifting activation of a cryptic splice site deleting seven nucleotides in exon 6. p.G64R reduced the expression of *DOK7* to 10% of wild-type *DOK7*, and markedly compromised AChR clustering in transfected C2C12 myotubes. p.G64R-*DOK7* made insoluble aggresomes at the juxtannuclear region in transfected C2C12 myoblasts and COS7 cells, which were co-localized with molecules in the autophagosome system. A protease inhibitor MG132 reduced the soluble fraction of p.G64R-*DOK7* and enhanced the aggresome formation of p.G64R-*DOK7*. To match the differentiation levels between patient-derived and control induced pluripotent stem cells (iPSCs), we corrected c.190G>A (p.G64R) by CRISPR/Cas9 to make isogenic iPSCs while retaining c.653-1G>C (CMS-iPSCs^{Cas9}). Myogenically differentiated CMS-iPSCs showed juxtannuclear aggregates of *DOK7*, reduced expression of endogenous *DOK7* and reduced phosphorylation of endogenous MuSK. Another mutation, p.T77M, also made aggresome to a less extent compared with p.G64R in transfected COS7 cells. These results suggest that p.G64R-*DOK7* makes aggresomes in cultured cells and is likely to compromise MuSK phosphorylation for AChR clustering.

Introduction

Congenital myasthenic syndromes (CMS) are a heterogeneous group of rare inherited diseases characterized by muscle weakness and fatigue resulting from compromised signal transduction at the neuromuscular junction (NMJ) (1). Mutations in a total of 34 genes have been reported to cause CMS (2,3). Molecules in the agrin-LRP4-MuSK-*DOK7* signaling pathway are essential for the clustering of acetylcholine receptors (AChRs) at the motor endplate (4–10). Both defective and excessive phosphorylation of muscle-specific kinase (MuSK) reduces AChR clusters (11). The downstream of tyrosine kinase 7 (*DOK7*) enhances agrin-triggered MuSK phosphorylation (8,9). In the absence of *Dok7* in mice, agrin cannot induce AChR clustering (12). Phosphorylated MuSK also recruits *DOK7* and induces *DOK7* phosphorylation. This positive feedback loop ensures sufficient activation of MuSK and triggers AChR clustering. *DOK7* is comprised of a pleckstrin homology (PH) domain, a phosphotyrosine-binding (PTB) domain and a long unstructured C-terminal region containing a nuclear exporting signal (NES) and two tyrosine residues that can be phosphorylated. The PH domain enables the anchoring of *DOK7*

to the plasma membrane and the assembly of a protein complex with MuSK (13). The PTB domain contains a MuSK-binding motif (9). The integrity of the PH-PTB domains is critical for dimerizing *DOK7* to facilitate MuSK phosphorylation (14). The NES domain controls the subcellular localization of *DOK7*. Two tyrosine residues provide binding sites for the adaptor proteins such as Crk and Crk-L (15,16), which mediate the downstream signaling pathway to induce AChR clustering at the NMJ.

DOK7 mutations account for 10–15% of CMS, and are the most common cause of limb-girdle myasthenia (8,15,17). More than 70 missense, truncation and splicing mutations have been reported in *DOK7* in CMS (8,15,17,18). Mutations in *DOK7* cause aberrantly small and simplified neuromuscular synapses (8). Patients with *DOK7* mutations usually respond to ephedrine or salbutamol, but often worsen with cholinesterase inhibitors that are effective in most types of CMS (19,20). Twelve missense mutations in *DOK7* (p.E3K, p.P31T, p.A33V, p.S45L, p.T77M, p.G109C, p.V139L, p.R158Q, p.G161R, p.G166R, p.G171D and p.G180A) have been characterized in overexpression systems in two reports (15,21). They variably reduced the phosphorylations of MuSK and AChR $\beta 1$ subunit, but

Received: July 22, 2022. Revised: December 12, 2022. Accepted: December 21, 2022

© The Author(s) 2022. Published by Oxford University Press.

This is an Open Access article distributed under the terms of the Creative Commons Attribution License (<https://creativecommons.org/licenses/by/4.0/>), which permits unrestricted reuse, distribution, and reproduction in any medium, provided the original work is properly cited.

none reduced the expression of DOK7. Formation of aggregates by mutant DOK7 has not been investigated to date.

Here, we characterized two mutations, c.653-1G>C and c.190G>A, in DOK7 in a patient with CMS (Fig. 1A and B). c.653-1G>C generated two aberrantly spliced transcripts in CMS-induced pluripotent stem cells (iPSCs). In transfected COS7 cells and C2C12 myoblasts/myotubes, p.G64R reduced the expression of DOK7 by forming insoluble aggregates, and compromised MuSK phosphorylation and AChR clustering. In CMS-iPSCs, p.G64R formed juxtannuclear aggregates to a less extent and reduced the expression of DOK7 and MuSK phosphorylation, which were rescued by correcting p.G64R by CRISPR/Cas9.

Results

CMS patient

A male patient, currently at age 24 years, had respiratory distress and muscle weakness at birth. He had undergone tracheotomy and was dependent on a respirator up to age 4 years. He had ptosis and limitations in eye movements, which disappeared over time, but the exact temporal profile was not recorded. At age 4 years, he started walking independently, but he showed marked day-to-day variability from being unable to walk to being able to climb 10 steps of stairs. He showed no diurnal fluctuation of muscle weakness. Currently, proximal dominant muscle weakness is observed, but the patient is able to walk independently. Repetitive nerve stimulation decreased the amplitude of compound muscle action potential to 79% of the accessory nerve, but not of the median nerve. Biopsy of biceps brachii at age 9 years showed a decrease of type IIB fibers and an increase of type IIC fibers, but no tubular aggregates. Ephedrine hydrochloride and 3, 4-diaminopyridine showed moderate effects.

Mutations in DOK7

Sanger sequencing revealed that the patient was heterozygous for two mutations in DOK7. One was c.190G>A (NM_173660.5) at position 3 473 495 (GRCh38/hg38) on chromosome 4, predicting p.G64R (NP_775931.3) in the PH domain (Fig. 1A and B). p.G64 is highly conserved across species (Fig. 1C). p.G64R was predicted to be highly pathogenic by InMeRF with a probability of 0.890 (22) (Supplementary Material, Table S1). p.G64R has an accession number of rs1246160310 in dbSNP with global minor allelic frequency (GMAF)=0.0011% (3/266842). p.G64R was previously reported in two unrelated CMS patients without functional characterization (23). p.G64 was located at the interface between the PH and PTB domains in dimerized DOK7 (Fig. 1D and E) (14).

Another mutation was c.653-1G>C (NM_173660.5) at position 3 491 403 (GRCh38/hg38) on chromosome 4, at the 3' end of intron 5 (Fig. 1A and B). c.653-1G>C has an accession number of rs1449351306 with GMAF=0.006% (1/16760). c.653-1G>C was reported in another DOK7-CMS patient without functional characterization (24).

Sanger sequencing showed that the asymptomatic father and mother were heterozygous for c.653-1G>C and c.190G>A, respectively.

Activation of a cryptic 3' splice site in DOK7 exon 6 due to c.653-1G>C at the 3' end of intron 5

To examine the effects of c.653-1G>C on splicing, we analyzed DOK7 transcripts in CMS-iPSCs (Fig. 1). Reverse transcription-polymerase chain reaction (RT-PCR) spanning DOK7 exon 6 (120 bp) and sequencing of cloned fragments showed two aberrantly spliced transcripts in CMS-iPSCs (Fig. 2A). One was

due to skipping of exon 6, and the other was due to an activation of a cryptic splice site deleting seven nucleotides at the 5' end of exon 6 (Fig. 2B and C). The exon 6-skipped transcript was more abundant than the 7-nt-deleted transcript.

The exon 6-skipped DOK7 transcript has an in-frame deletion lacking codons 218–257 (p.D218_G257del), where the nuclear export signal (NES) at 240–249 is located (Fig. 2D). Although p.D218_G257del-DOK7 was similarly expressed compared with WT-DOK7 in COS7 cells (Fig. 2E), disruption of the NES domain was previously reported to compromise MuSK phosphorylation and impair AChR clustering in C2C12 myotubes (15,25). The 7-nt-deleted transcript (c.653_659delACCCAAG) predicts p.D218Afs*34 (Fig. 2D), the expression level of which was markedly reduced in COS7 cells (Fig. 2E). These results suggested that c.653-1G>C was likely to generate DOK7 with markedly compromised functions.

Effects of p.G64R on protein expression and AChR clustering

First, we analyzed the expression level of p.G64R-DOK7. Western blotting of transfected C2C12 myoblasts showed that p.G64R significantly reduced the expression of DOK7 (Fig. 3A). Second, we examined the binding of DOK7 to MuSK and the phosphorylation of MuSK. As C2C12 myotubes express DOK7 endogenously, we used COS7 cells that express no or negligible amounts of DOK7 and MuSK (15). p.G64R had no effect on the protein level of MuSK, but reduced the amount of MuSK co-immunoprecipitated with DOK7 in COS7 cells that were transfected with FLAG-tagged MuSK along with WT-DOK7 or p.G64R-DOK7 (Supplementary Material, Fig. S1A). Similarly, tyrosine phosphorylation of MuSK was markedly reduced in p.G64R-DOK7-transfected COS7 cells (Supplementary Material, Fig. S1A). Third, we analyzed the effects of p.G64R on AChR clustering using C2C12 myotubes. WT-DOK7 induced AChR clustering in the absence of agrin, but p.G64R-DOK7 had no essential AChR clustering activity in transfected C2C12 myotubes (Fig. 3B and C). These results suggested that p.G64R reduced the expression of DOK7, and compromised the DOK7-mediated MuSK phosphorylation and AChR clustering.

Ubiquitin inhibitor MG132 accelerates the reduction of soluble p.G64R-DOK7 through forming insoluble aggregates

We next examined whether the reduced expression of p.G64R-DOK7 was due to (i) the reduced amount of mRNA, (ii) the accelerated degradation of DOK7 [e.g. degradation by the ubiquitination proteasome system (UPS)] or (iii) the formation of detergent-insoluble aggregates. First, quantitative RT-PCR of DOK7 transfected into COS7 cells showed that WT- and p.G64R-DOK7 were similarly transcribed, and the addition of a proteasome inhibitor, MG132, had no effect on mRNA levels (Supplementary Material, Fig. S1B). Second, treatment of transfected COS7 cells with MG132 for 3 h decreased the amount of p.G64R-DOK7 (Fig. 4A) in a dose-dependent manner with an apparent half-life of 3.3 h (Supplementary Material, Fig. S1C and D). This indicated that an accelerated UPS-mediated degradation of DOK7 was not the cause of the reduced expression of p.G64R-DOK7. Third, we examined whether p.G64R form a detergent-insoluble fraction. WT-DOK7 was mostly present in the detergent-soluble fraction, whereas p.G64R-DOK7 was mostly located in the detergent-insoluble fraction (Fig. 4B). p.G64R also decreased the sum of the soluble and insoluble fractions of DOK7 (Fig. 4C). MG132 treatment increased the amount of p.G64R-DOK7 in the insoluble fraction in dose- and time-dependent manners (Fig. 4D and E). Immunostaining of

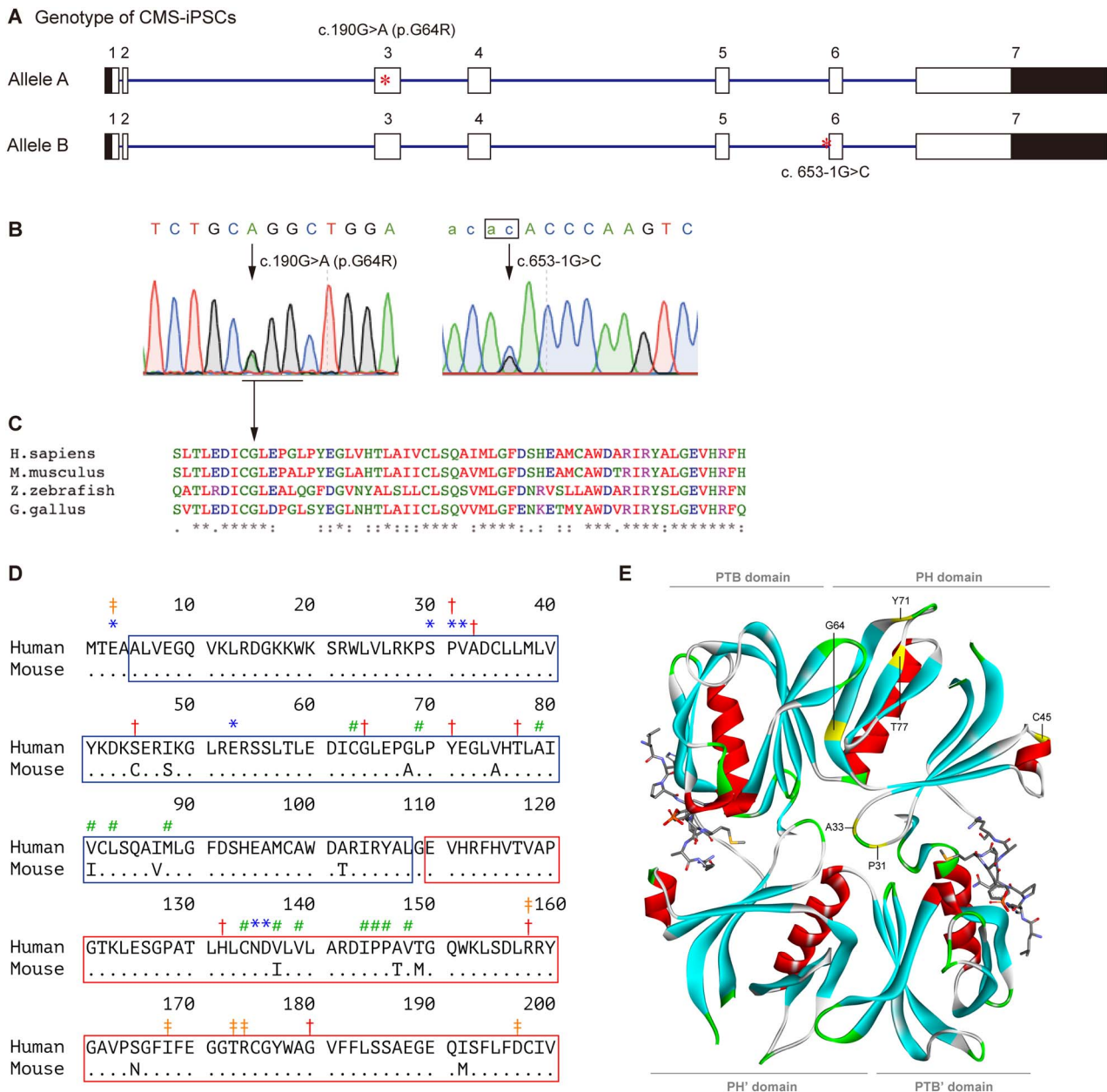


Figure 1. Mutations in *DOK7*. (A) Schematic of *DOK7* gene (NM_173660.5) showing the location of mutations (red asterisks). The 5' and 3' untranslated regions are shown in black. (B) Sequencing chromatograms showing heteroallelic mutations. An invariant 'ag' dinucleotide at the 3' end of intron 5 is indicated by a box. (C) Alignment of *DOK7* proteins across species. Alignment was performed using ClustalW2 (<https://www.ebi.ac.uk/Tools/msa/clustalw2/>). Glycine at codon 64 (GGG) is conserved across species, and is changed to arginine (AGG). (D) Alignment of the PH (blue box) and PTB (red box) domains of human and mouse *DOK7* (14). Identical residues are indicated by dots. *Residues for *DOK7* dimerization. #Residues for PH-PTB interaction. ‡Residues for binding to MuSK pTyr533. †Residues mutated in CMS. Note that the mutated serine at codon 45 in human is cysteine at codon 45 in mouse. (E) Crystal structure of the PH and PTB domains of mouse *DOK7* dimer (ribbons) and MuSK phosphopeptides (sticks) (14). Six residues mutated in CMS in the PH domain are indicated in the upper *DOK7*. Domains in the lower *DOK7* are indicated by apostrophe.

DOK7 in COS7 cells expressing WT- and p.G64R-*DOK7* also showed that p.G64R-*DOK7* was prone to form aggregated puncta at the juxtannuclear region, whereas WT-*DOK7* was diffusely dispersed in the cytoplasm (Fig. 4F and G). Thus, p.G64R-*DOK7* that could not be degraded by the UPS was sequestered into the insoluble fraction, which subsequently reduced the expression of p.G64R-*DOK7*.

In addition to COS7 cells, we also evaluated the aggregates of p.G64R-*DOK7* in transfected C2C12 myoblasts. We observed that enhanced green fluorescent protein (EGFP)-fused p.G64R-*DOK7* formed aggregates at the juxtannuclear region in C2C12 myoblasts (Supplementary Material, Fig. S2). Addition of the PLC lysis buffer to transfected C2C12 myoblasts dispersed the

cytoplasmic green signals of WT-*DOK7*-EGFP, but not of aggregates made of p.G64R-*DOK7*-EGFP, indicating that the aggregates were detergent-insoluble (Supplementary Material, Video).

These results suggested that the reduced expression of p.G64R-*DOK7* was accounted for by the formation of abnormal aggregates at the juxtannuclear region.

Characterization of aggregates formed by p.G64R-*DOK7*

The UPS is primarily responsible for eliminating unfolded and misfolded proteins. When the load of UPS is overwhelmed, protein aggregates are formed at the microtubule-organizing center (MTOC) in a microtubule-dependence manner (26). We

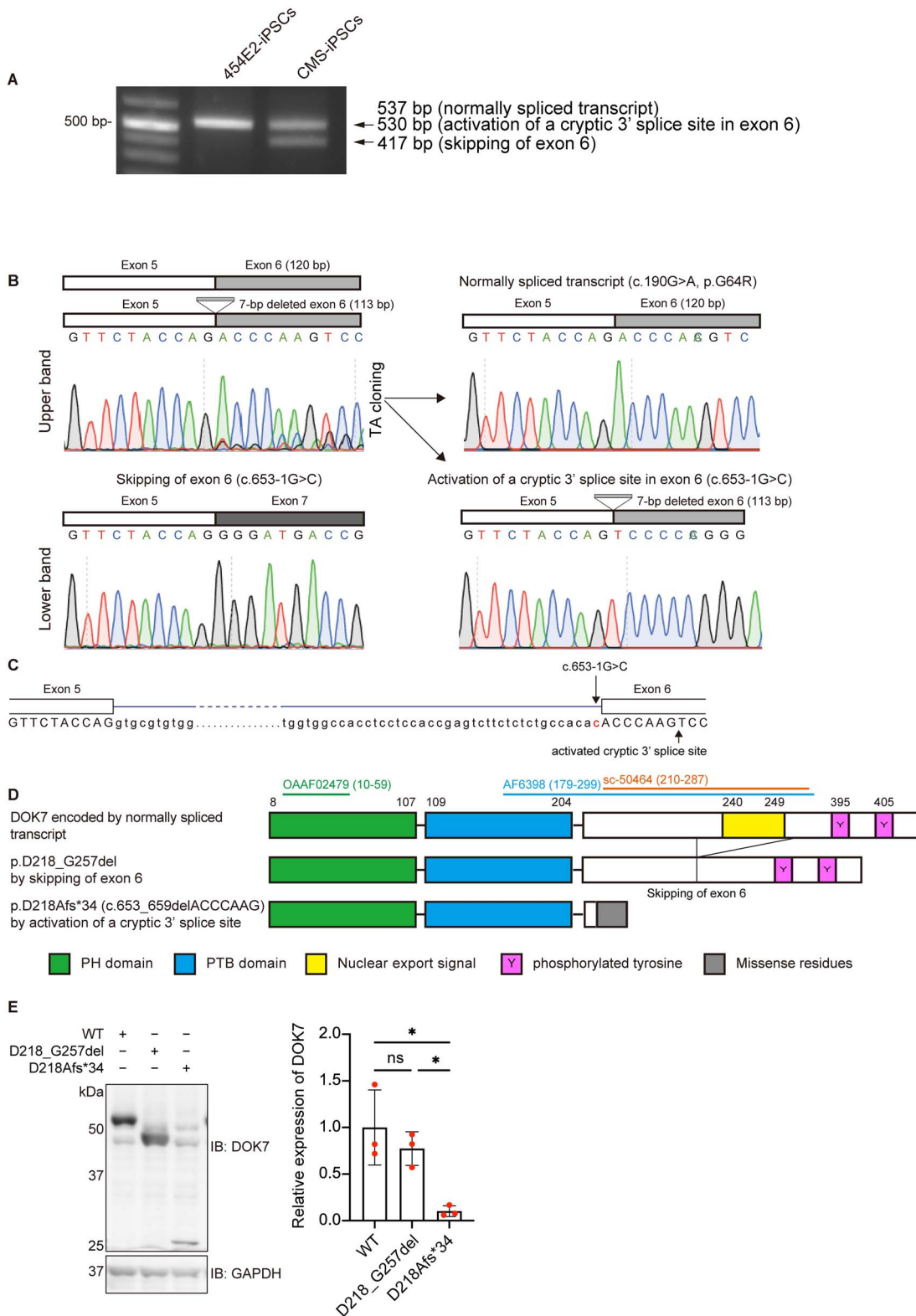


Figure 2. Aberrantly spliced transcripts due to c.653-1G > C. **(A)** RT-PCR spanning *DOK7* exon 6 of control 454E2-iPSCs and patient-derived CMS-iPSCs. The upper band was comprised of 537-bp and 530-bp fragments. **(B)** Sequence chromatograms of three RT-PCR products in CMS-iPSCs. Chromatograms of the two transcripts in the upper band in A are indicated on the right. **(C)** Schematic showing the positions of the c.653-1 > C mutation and activated cryptic 3' splice site that is seven nucleotides downstream of the intron 5/exon 6 junction. **(D)** Schematic presentation of *DOK7* proteins encoded by three transcripts in B. Epitopes of three *DOK7* antibodies (OAAF02479, AF6398 and sc-50464) used in this study are indicated with codon numbers in parentheses. See [Supplementary Material, Table S2](#) for the details of these antibodies and [Supplementary Material, Fig. S5A](#) for representative western blotting. **(E)** Representative western blotting and quantitative analysis of mutant *DOK7* arising from an allele with c.653-1G > C in transfected COS7 cells. Expression levels were normalized to that of GAPDH and to the ratio of wild-type (WT) *DOK7*. Mean and SD (n = 3 experiments) are indicated with individual values in red dots. One-way ANOVA with Dunnett's post hoc multiple comparison test was applied (ns, no significance; *P < 0.05).

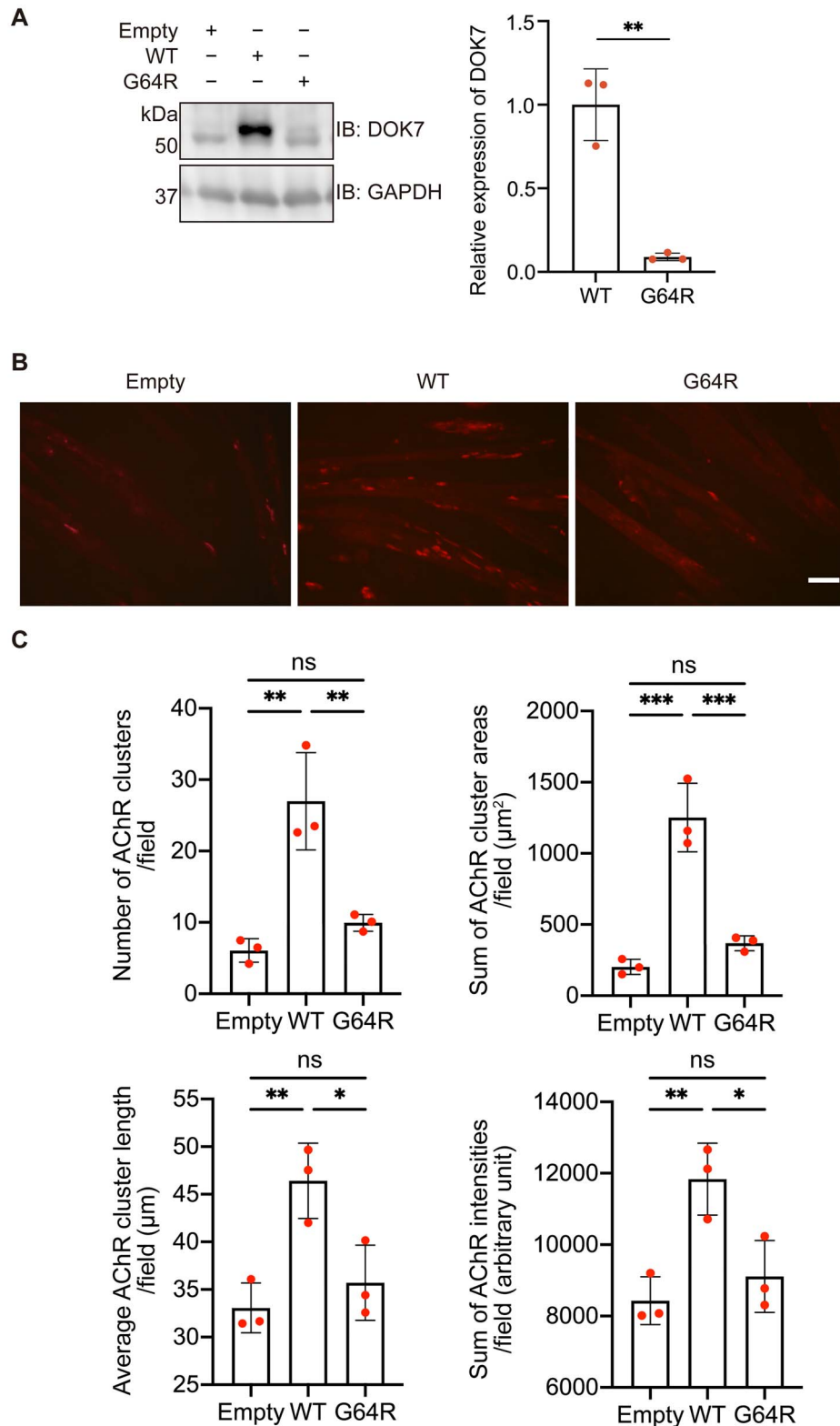


Figure 3. Effects of p.G64R-DOK7 on protein expression and AChR clustering in C2C12 cells. **(A)** Representative western blotting and quantitative analysis of DOK7 in C2C12 cells transfected with wild-type (WT)-DOK7 or p.G64R-DOK7. Mean and SD ($n = 3$ experiments) are indicated with individual values in red dots. Student's *t*-test (** $P < 0.01$). **(B)** Transfection of wild-type (WT)-DOK7 but not p.G64R-DOK7 induced AChR clustering visualized by Alexa 594-conjugated α -bungarotoxin (red) in C2C12 cells without agrin. Scale bar = 50 μm . **(C)** Quantitative analysis of the number, total area, average length and total signal intensity per visual field (0.143 mm^2) of AChR clusters in C2C12 cells expressing WT-DOK7 or p.G64R-DOK7. p.G64R-DOK7 markedly reduced AChR clustering. The mean values of 30 visual images are indicated by red dots. One-way ANOVA and Dunnett's multiple comparison test (ns, no significance; * $P < 0.05$, ** $P < 0.01$ and *** $P < 0.001$).

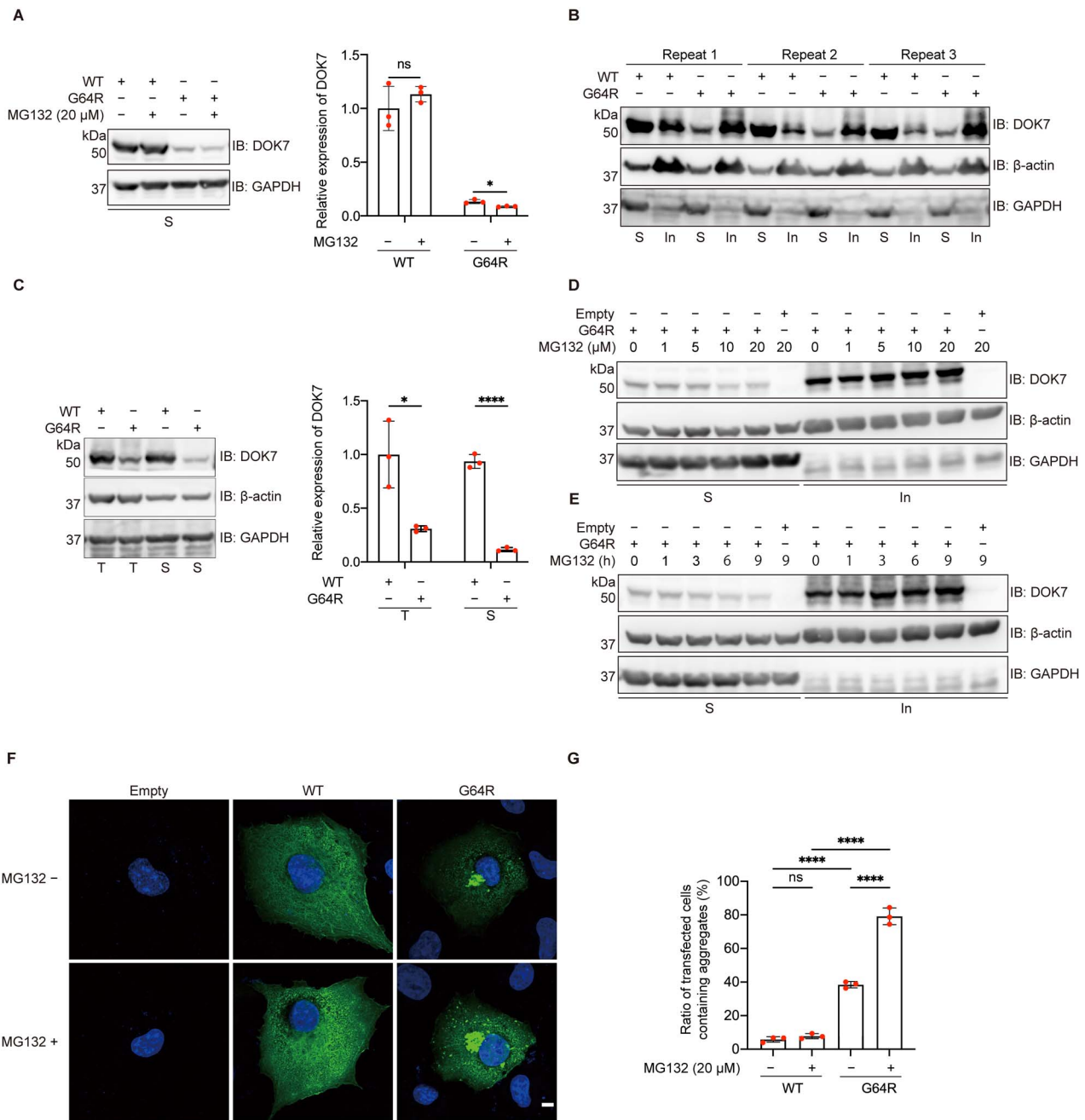


Figure 4. Effects of p.G64R-DOK7 on protein solubility. (A and C) Representative western blotting and quantitative analysis of DOK7 and GAPDH without β -actin (A) or with β -actin (C) in detergent-soluble fractions (S) and total protein lysates (T), in transfected COS7 cells. MG132 (20 μ M) was added 3 h before harvesting cells (A). Expression levels were normalized to that of GAPDH, and also to the ratio of wild-type (WT)-DOK7. Mean and SD ($n = 3$ experiments) are indicated with individual values in red dots. Multiple Student *t*-test was applied (ns, no significance, $*P < 0.05$, $****P < 0.0001$). Triplicated (B) and representative (D and E) western blotting of DOK7, β -actin and GAPDH in detergent-soluble (S) and insoluble (In) fractions, in transfected COS7 cells. (D) MG132 at 0–20 μ M was added 3 h before harvesting cells. (E) MG132 at 20 μ M was added at indicated time points. (F) Representative images of WT-DOK7 and p.G64R-DOK7 treated with or without 20 μ M MG132 treatment for 3 h in transfected COS7 cells. Green and blue signals represent DOK7 and DAPI, respectively. Scale bar = 10 μ m. (G) The ratio of transfected COS7 cells with aggregates in each experiment is indicated in red dot. Each experiment is an average of five visual fields and is comprised of at least 100 cells. Mean and SD ($n = 3$ experiments) are indicated. One-way ANOVA with Dunnett's multiple comparison test (ns, no significance; $****P < 0.0001$).

thus examined the association of the aggregates with molecules in the MTOC. Nocodazole, an inhibitor of microtubule formation, markedly reduced the formation of aggresomes of p.G64R-DOK7 in transfected COS7 cells (Fig. 5A). A microtubule component, α -tubulin (Fig. 5B) as well as the other aggresome markers (ubiquitin, parkin, P62, and HSP70) (Fig. 5C–F) were colocalized with p.G64R-DOK7 aggregates. These results suggested that p.G64R caused abnormal folding of DOK7, which made DOK7

ubiquitinated, transported to MTOC and form aggresomes at the juxtannuclear region.

Comparison of CMS-iPSCs with p.G64R and isogenic CMS-iPSCs^{Cas9} without p.G64R

To dissect the effect of p.G64R in patient-derived iPSCs, we established an isogenic cell line, CMS-iPSCs^{Cas9}, from CMS-iPSCs

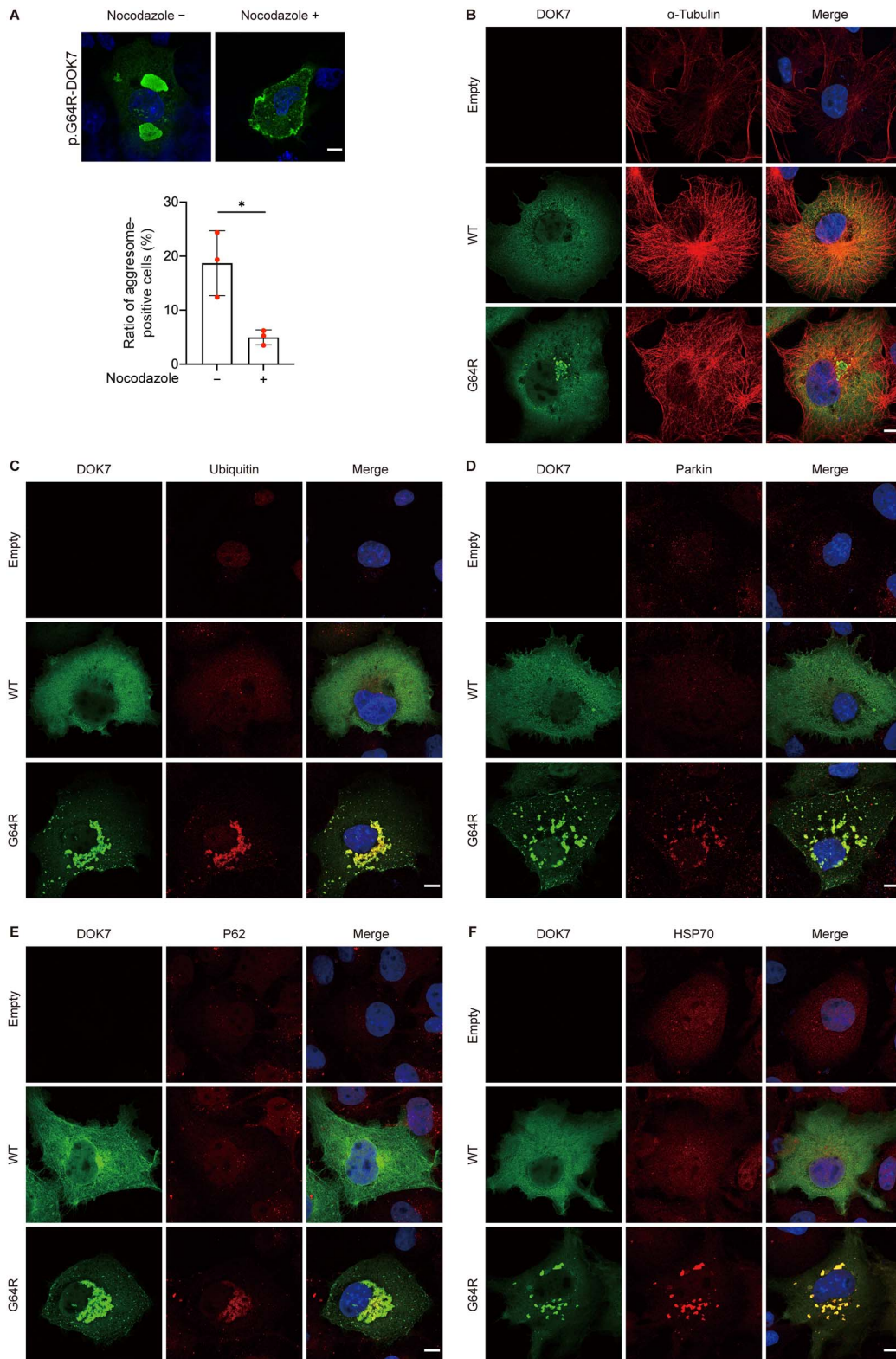


Figure 5. Characterization of aggregates of p.G64R-DOK7. **(A)** Representative immunostaining of p.G64R-DOK7 in transfected COS7 cells with or without $10 \mu\text{M}$ nocodazole, an inhibitor of microtubule polymerization. Scale bar = $10 \mu\text{m}$. The ratio of aggresome-positive cells after $10 \mu\text{M}$ nocodazole treatment for 3 h in five visual fields is plotted in red for each experiment. Mean and SD ($n = 3$ experiments) are indicated. $*P < 0.05$ by Student's *t*-test. **(B-E)** Colocalization of DOK7 and aggresome markers of α -tubulin (B), ubiquitin (C), parkin (D), P62 (E) and HSP70 (F). COS7 cells transfected with wild-type (WT)-DOK7 or p.G64R-DOK7 were immunostained with indicated antibodies at 18 h after transfection. Scale bar = $10 \mu\text{m}$.

by correcting c.190A > G (p.G64R), while retaining c.653-1G > C on another allele (Supplementary Material, Fig. S3A–C). First, myogenic marker genes (*MYH3* and *MYOD1*) and NMJ-associated genes (*LRP4*, *DOK7*, *MUSK* and *CHRNG*) were induced in myogenic differentiation of both CMS-iPSCs and CMS-iPSCs^{Cas9} (Supplementary Material, Fig. S3D). Next, we observed that, in contrast to CMS-iPSCs^{Cas9}, endogenous *DOK7* was undetectable even after immunoprecipitation (Fig. 6A), and the phosphorylation of endogenous *MuSK* was markedly low in myogenically differentiated CMS-iPSCs (Fig. 6B and Supplementary Material, Fig. S4A). Although the staining of endogenous *DOK7* was markedly weak in myogenically differentiated CMS-iPSCs (Supplementary Material, Fig. S4B), *DOK7* made aggregates at the juxtannuclear region (Fig. 6C and D). In contrast to COS7 cells, however, *HSP70* was not colocalized with *DOK7*. Taken together, p.G64R reduced the expression of *DOK7* and *MuSK* phosphorylation and formed aggregates at the juxtannuclear region in myogenically differentiated CMS-iPSCs.

Unavailability of two anti-*DOK7* antibodies, where one was for immunoprecipitation and the other was for immunoblotting, prevented us from evaluating abnormal *DOK7* originating from an allele with c.653-1G > C in CMS-iPSCs (Supplementary Material, Fig. S5 and Supplementary Material, Table S2).

Prediction and observation of aggresome formations by five missense mutations at the PH domain

As shown in Figure 1D and E, six missense mutations (p.P31T, p.A33V, p.S45L, p.G64R, p.Y71F and p.T77M) have been reported in CMS at the PH domain. Except for p.S45L that was not conserved between mouse and human (Fig. 1D), the effects of five missense mutations on protein stability and protein structure were evaluated by eight tools (Supplementary Material, Table S3a). Among the five missense mutations, $\Delta\Delta G$ of p.G64R, which is a hallmark of the effect on the protein instability (27,28), was ranked first or second in most tools (Supplementary Material, Table S3b). Generation of novel aggregation-prone regions (APRs) by p.G64R was also predicted (Supplementary Material, Fig. S6A and B). In addition, substantial structural changes of p.G64R, as well as p.T77M to a less extent, were predicted (Supplementary Material, Table S3c). Furthermore, p.G64R was predicted to form new interactions with other amino acids (Supplementary Material, Fig. S6C). We indeed observed that, among the five missense mutations, p.T77M also formed juxtannuclear aggresome to a less extent compared with p.G64R (Fig. 7), but the expression level of p.T77M was not reduced. Thus, the formation of aggresome is not unique to p.G64R-*DOK7*, and p.T77M can also disrupt *DOK7* folding and form aggresome.

Discussion

We identified compound heterozygous mutations (c.653-1G > C and p.G64R) in *DOK7* in a patient with CMS. *DOK7*-CMS is classified into limb-girdle myasthenia, but a review of 15 patients with *DOK7*-CMS showed the presence of ocular involvement in 11 patients (73%) (29), as we observed in our patient. The deletion of the C-terminal region of *DOK7* in one or two alleles is observed in most *DOK7*-CMS patients, which markedly reduces the expression levels of *DOK7* (18). In addition, the deletion of the C-terminal region and the disruption of the NES domain in *DOK7* compromise *DOK7*-mediated *MuSK* phosphorylation and impair AChR clustering in C2C12 myotubes (15,25). We also observed that the C-terminal truncated *DOK7* by c.653-1G > C markedly reduced the protein expression level. In contrast to *Dok7*-deficient mice that

showed no AChRs in the diaphragm (2,3), mice carrying the PH and PTB domains by knocking in homozygous c.1124_1127dupTGCC can form immature AChRs with small size, less number and simplified structure (30). Similarly, *DOK7*-CMS patients with homozygous c.1124_1127dupTGCC show severe symptoms but are not lethal (30). Therefore, lack of the C-terminal region of *DOK7* largely compromises the NMJ formation, but does not nullify the effect of *DOK7*.

We observed that un- or mis-folded p.G64R-*DOK7* caused an overload to the UPS, and unprocessed p.G64R-*DOK7* made aggresomes at the MTOC. Similar activation of the autophagosome system by an overload the UPS has been repeatedly reported and is reviewed (26). Myogenically differentiated CMS-iPSCs showed that *DOK7* made aggregates at the juxtannuclear region without colocalization of *HSP70* and that *DOK7* expression and *MuSK* phosphorylation were markedly reduced. CRSPR/Cas9-mediated correction of p.G64R in CMS-iPSCs rescued these phenotypes. Lack of aggresomes in CMS-iPSCs was likely to be accounted for by high UPS activities in iPSCs (31–33). Alternatively, this was due to a technical constraint that iPSCs could not form mature myotubes compared with C2C12 myoblasts (34). Although aggresomes were observed in cultured cells and possibly in CMS-iPSCs, no aggregates were observed by hematoxylin-eosin (HE) staining of biopsied skeletal muscle at Age 9, and the disease did not progress in 15 years after the biopsy, the roles of aggresomes in the patient remain elusive.

Small molecule chaperones, cystic fibrosis transmembrane conductance regulator (CFTR) correctors, have been successfully applied to and approved for reverting folding defects of the CFTR- $\Delta F508$ mutant in cystic fibrosis (35–37). CFTR correctors are unique in that most small molecule chaperones were developed as competitive inhibitors, whereas CFTR correctors enhance protein folding (38). Similar small molecule chaperons may be able to correct misfolding of mutant *DOK7* due to p.G64R and others.

Materials and Methods

Generation of CMS-iPSCs

CMS-iPSCs were generated from the peripheral blood monocytes of a patient. All clones were generated using episomal vectors as previously described (39,40). Control iPSCs (454E2-iPSCs) were obtained from the Center for iPS Cell Research and Application, Kyoto University. The established CMS-iPSCs and 454E2-iPSCs were cultured in Primate ES Cell medium (RCHEMD001, Repro CELL) supplemented with 8 ng/ml basic fibroblast growth factor (RCHEOT003, Repro CELL) and 1× Zell Shield (13-0050, Minerva Biolabs) on mitomycin C-treated SNL feeder cells, as described previously (41). For establishment of feeder-free culture of iPSCs, feeder-dependent cultures were adapted into Essential 8 Flex medium (E8-Flex, A28585, Thermo Fisher Scientific) according to the manufacturer's protocol. For passaging, the cells were treated with 1 mg/ml Collagenase IV solution (C4-28, Sigma-Aldrich) and gravity-sedimented. The cells were then suspended in E8-Flex and distributed on vitronectin-(VTN-N, A14700, Thermo Fisher Scientific) coated dishes containing E8-Flex medium with 10 μ M Y-27634. For differentiation into skeletal muscle cells, doxycycline (Dox)-inducible *MyoD* expression vector and *PBase* vector were electroporated into CMS-iPSCs and 454E2-iPSCs using a NEPA21 type II electroporator (Nepa Gene) (42). The transduced cells were selected with puromycin (P8833, Sigma-Aldrich) (1 μ g/ml for CMS-iPSCs or 125 ng/ml for 454E2-iPSCs) and clones showing uniformly high *MYOD1* expression were selected. The gene expressions of pluripotency markers, *POU5F1* (Oct3/4), *SOX2*, *NANOG* and *MYC*

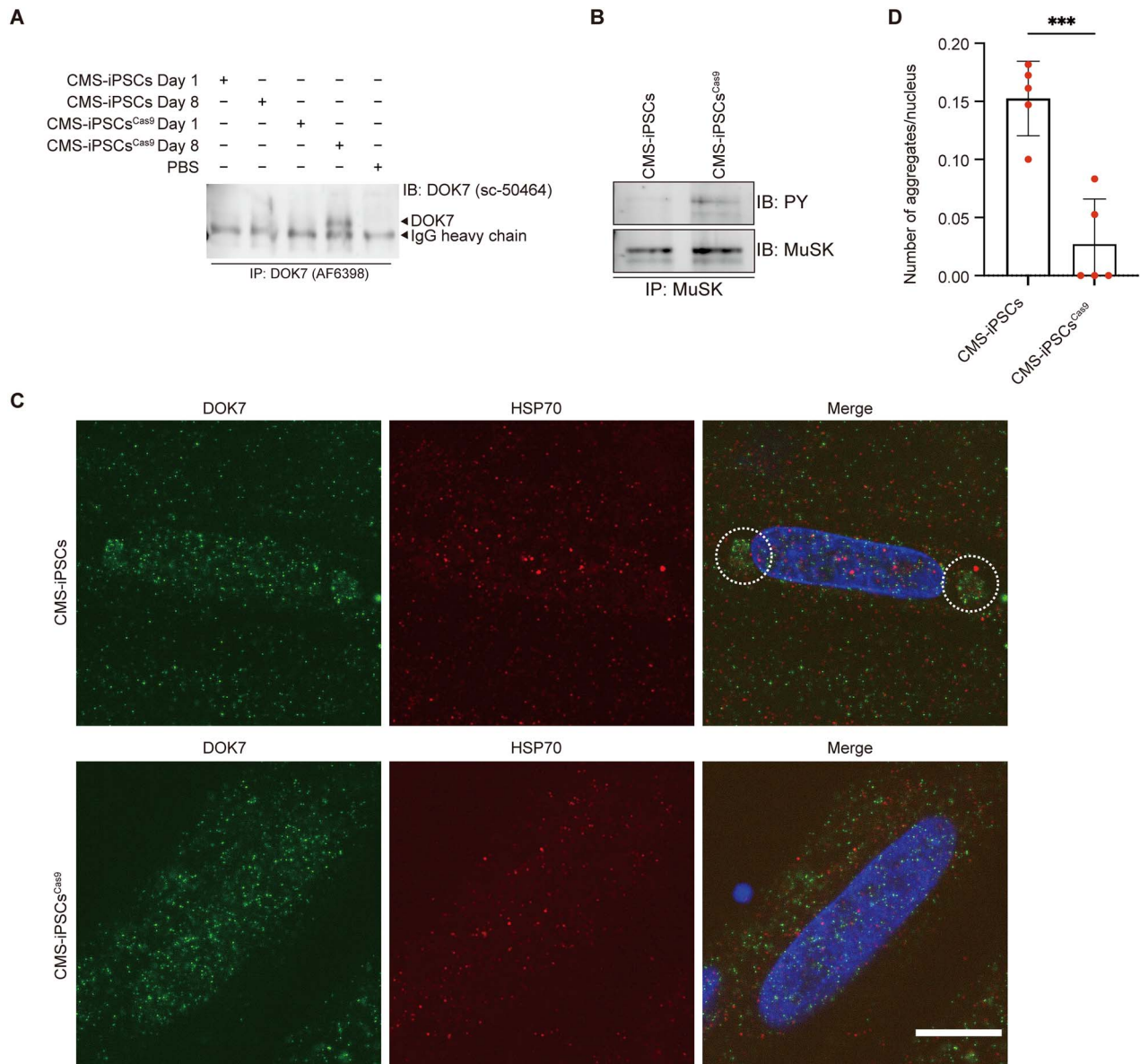


Figure 6. The expression level of DOK7, the phosphorylation of MuSK and the formation of aggregates in patient-derived CMS-iPSCs and isogenic CMS-iPSC^{Cas9}. **(A)** Representative western blotting of DOK7 in myogenically differentiated iPSCs on Day 8. Low expression level of DOK7 necessitated the enrichment of DOK7 by immunoprecipitation (IP) before immunoblotting (IB). Anti-DOK7 antibodies are indicated in parentheses. **(B)** Phosphorylated MuSK was immunoblotted (IB) by an anti-phosphotyrosine antibody (PY) after immunoprecipitation (IP) of MuSK. **(C)** Representative immunostaining of DOK7 and HSP70 in CMS-iPSC- and CMS-iPSC^{Cas9}-derived myogenic cells. Juxtannuclear aggregates are indicated by dotted circles. Scale bar = 10 μ m. **(D)** The number of juxtannuclear aggregates was blindly counted in five visual fields (~30 nuclei each). Mean and SD are plotted. *** $P = 0.005$ by Student's t-test.

(c-myc) were detectable in undifferentiated CMS-iPSCs and 454E2-iPSCs by RT-PCR (Supplementary Material, Fig. S8A). After 8 days of myogenic differentiation, myotube-like spindle-shaped cells with multiple nuclei were observed (Supplementary Material, Fig. S8B and C). There was no significant difference in the morphology in both clones.

Generation of isogenic control CMS-iPSCs^{Cas9}

Genomic sequences of *DOK7* exons 3 and 6 in CMS-iPSCs were first determined by Sanger sequencing to confirm the presence of heterozygous c.653-1G > C and c.190G > A mutations. To make isogenic control iPSCs, c.190G > A (p.G64R) in *DOK7* exon 3 in CMS-iPSCs was corrected by CRISPR/Cas9 in an allele-specific manner (Supplementary Material, Fig. S9), while retaining c.653-1G > C on another allele. The guide RNA (gRNA) was designed against

allele A carrying c.190G > A using CHOPCHOP (<https://chopchop.cbu.uib.no/>). The c.190G > A mutation was located 4 bp upstream of the protospacer adjacent motif (PAM) site. The sequence of an 81-nt single-strand oligodeoxynucleotide (ssODN) was: 5'-CCAGCGTGTGGACCAGGCCCTCGTAGGGCAGGCCGGGCTcAGCCcGCAGATGTCCTCTAGCGTCAGGCTGCTGCGTCCCC-3', where the complementary sequence shown in Supplementary Material, Fig. S8A is underlined. The ssODN carried c.190G to correct the mutation (lowercase letter 'c'), as well as an artificial silent c.195G > C mutation (lowercase letter 'g') at the PAM site, which also introduced an XhoI restriction site. Cas9 protein (Thermo Fisher Scientific), gRNA and ssODN were introduced into iPSCs by electroporation following a previously reported protocol (43). Electroporated cells were cultured in two dishes. At 48 h after transfection, DNA was extracted from a single dish, and a PCR

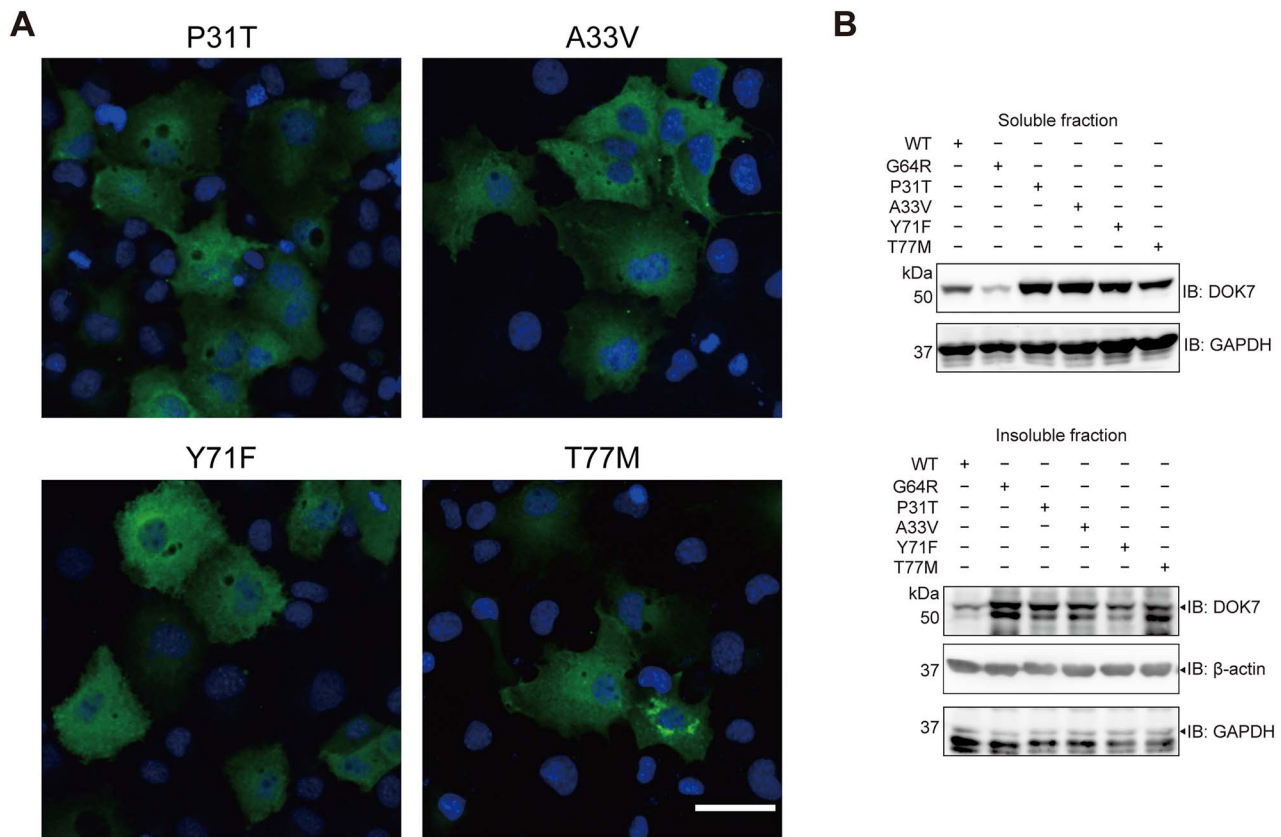


Figure 7. Immunostaining and western blotting of four other missense mutants at the PH domain of DOK7 in COS7 cells. **(A)** Representative immunostaining of DOK7 in COS7 cells transfected with indicated mutants. Refer to Figure 4I for representative images of wild-type and p.G64R-DOK7. Scale bar = 50 μm . **(B)** Western blotting of DOK7 in soluble (upper) and insoluble (lower) fractions in transfected COS7 cells.

fragment spanning c.190G > A was digested by *XhoI* to confirm the presence of cells carrying the artificial silent mutation. Next, 200–400 cells were plated on a 10-cm dish for isolation of single colonies for 7–10 days. Single colonies were picked up, and further expanded in 48-well plates. Mutation-corrected cells (CMS-iPSCs^{Cas9}) were identified by an allele-specific PCR (ASP) primer, 5'-GCCTGACGCTAGAGGACATCTGGcGGgTc-3', where 'g' at position -6 was for recognizing the corrected c.190G, 'g' at position -3 was an artificial mismatch against the target cDNA for better discrimination in ASP and 'c' at the 3' end was at the artificial silent mutation at the PAM site (Supplementary Material, Table S3). For ASP-positive colonies, the top five off-target sites, which were predicted by CHOPCHOP (<https://chopchop.cbu.uib.no/>), were Sanger-sequenced, and no artificial mutation was observed. We confirmed that CMS-iPSCs^{Cas9} had the expected correction (Supplementary Material, Fig. S3A), and expressed all pluripotency markers as in CMS-iPSCs (Supplementary Material, Fig. S3B). There were no significant differences in morphology during the myogenic differentiation (Supplementary Material, Fig. S3C).

Culture of CMS-iPSCs

iPSCs were cultured on a plate coated with Vitronectin (VTN-N, A14700, Thermo Fisher Scientific) in Essential-8 Medium (E8, A2858501, Thermo Fisher Scientific) containing puromycin (1 $\mu\text{g}/\text{ml}$ for CMS-iPSCs or 125 ng/ml for 454E2-iPSCs) and 10 μM Y-27632 (030-24 021, Fujifilm Wako Chemicals). Cells were seeded at a density of 14 000 cells per well in a 6-well plate and passaged every 5–7 days using Accutase (A1110501, Thermo Fisher Scientific). Medium was changed every day.

For myogenic differentiation, the cells were collected with Accutase, and seeded on a plate coated with Matrigel (Corning) in E8 with puromycin and Y-27632 (Supplementary Material, Fig. S7). On the next day (differentiation Day 1), the medium was replaced with Dulbecco's-modified Eagle's medium (DMEM)/F12 (11320 033, Thermo Fisher Scientific) supplemented with 5% KnockOut Serum Replacement (KSR, 10828028, Thermo Fisher Scientific), 10 μM SB431542 (SB, 13031, Cayman Chemical), 2 μM dorsomorphin (Dor, 3093, R&D Systems), 0.5 mM N-acetyl-L-cysteine (NAC, A7250, Sigma-Aldrich) and 3 μM CHIR99021 (CH, R&D Systems). At 24 additional hours (differentiation Day 2), the medium was changed to DMEM/F12 containing 5% KSR, SB, Dor, NAC and 1 μM retinoic acid (RA, R2625, Sigma-Aldrich). On differentiation Day 3, the medium was changed to DMEM/F12 with 5% KSR and 1 $\mu\text{g}/\text{ml}$ Dox. On differentiation Day 4, the medium was changed to Minimum essential medium α (αMEM) (2144 405, Nacalai Tesque) with 5% KSR, 100 μM 2-mercaptoethanol (2-ME) and 1 $\mu\text{g}/\text{ml}$ Dox. On differentiation Day 5, the medium was changed to the fresh αMEM . On differentiation Day 6, cells were dissociated with Accutase and seeded on Matrigel-coated plates at a density of 1.0×10^6 cells per well in a 6-well plate in αMEM , 5% KSR, 100 μM 2-ME and 1 $\mu\text{g}/\text{ml}$ Dox. On differentiation Day 7, cells were added with fresh medium with the same ingredients and were cultured for additional 24 h.

Transcriptomic and immunostaining analysis of CMS-iPSCs

Splicing pattern due to the c.653-1G > A mutation was determined by Sanger sequencing of transcripts spanning DOK7 exon 6. Primer sequences are shown in Supplementary Material, Table S4. For

immunofluorescent staining of DOK7 in CMS-iPSCs, 1.0×10^6 cells were plated on Matrigel-coated glass coverslips in each well of 6-well plate.

Analysis of AChR clustering in C2C12 myotubes transfected with wild-type and mutant DOK7

C2C12 myoblasts were cultured in DMEM supplemented with 10% fetal bovine serum (Thermo Fisher Scientific) at 37°C with 5% CO₂. One day before transfection, 1.0×10^5 cells were plated in each well of a collagen I-coated 6-well plate. On the following day, a plasmid encoding WT-DOK7 or p.G64R-DOK7 was transfected into C2C12 cells using lipofectamine 3000 (Thermo Fisher Scientific) according to the manufacturer's instructions. After 24 h, the medium was switched to DMEM with 2% horse serum (Thermo Fisher Scientific) to induce myogenic differentiation. After 5–7 days of differentiation, agrin (10 ng/ml) was added to induce AChR clustering for 18 h. To observe AChR clusters, cells were incubated with Alexa Fluor 594-tagged α -bungarotoxin for 1 h. Then, cells were fixed for 10 min using phosphate-buffered saline (PBS) containing 4% formaldehyde. Images were captured under an Olympus XL71 fluorescence microscope. The number, size and signal intensity of AChR clusters were analyzed using Image J software (<http://imagej.nih.gov/ij/>) with an automated macro (Supplementary Material, Fig. S10).

Analysis of detergent-soluble and insoluble fractions

Detergent-soluble and insoluble fractions were extracted as described previously with minor modifications (44). Briefly, cells were lysed in 60 μ L PLC buffer supplemented with protease inhibitors. After rotation at 4°C for 30 min, the lysates were centrifuged for 5 min at $15\,000 \times g$ at 4°C. The supernatants were designated as detergent-soluble proteins and transferred to new tubes. The pellets containing detergent-insoluble proteins were washed with PLC buffer and dissolved in 60 μ L urea buffer (2% SDS, 6 M urea and 30 mM Tris-HCl pH 7.6), followed by sonication on ice for 10 s. Equal volumes of protein extraction were heated at 95°C for 5 min in 2 \times Laemmli buffer and analyzed by western blotting.

Statistical analysis

Values are represented by mean and SD. Data were analyzed by Student's t-test, multiple Student's t-test or one-way ANOVA followed by Dunnett's posthoc test. P-values < 0.05 were considered to be statistically significant.

Genomic sequencing of the patient

Details are indicated in [Supplementary Materials and Methods](#).

Expression analysis of wild-type and mutant DOK7 in COS7 cells

Details are indicated in [Supplementary Materials and Methods](#).

Coimmunoprecipitation

Details are indicated in [Supplementary Materials and Methods](#).

Plasmid constructions

Details are indicated in [Supplementary Materials and Methods](#).

mRNA expression analysis by reverse-transcription PCR (RT-PCR) and real-time RT-PCR

Details are indicated in [Supplementary Materials and Methods](#).

Western blotting

Details are indicated in [Supplementary Materials and Methods](#).

Immunofluorescence staining and confocal microscope

Details are indicated in [Supplementary Materials and Methods](#).

Supplementary Material

Supplementary Material is available at HMG online.

Acknowledgements

We would like to acknowledge members at the Core Facility of Nagoya University Graduate School of Medicine for their technical support.

Conflict of Interest statement. None declared.

Funding

This study was supported by Grants-in-Aid from the Japan Agency for Medical Research and Development (JP22bm0804005 and JP22ek0109488), the Japan Society for the Promotion of Science (JP20H03561, JP21K06392 and JP21H04815); the Ministry of Health, Labour and Welfare of Japan (20FC1036) and the National Center of Neurology and Psychiatry (2–5).

References

- Engel, A.G., Shen, X.M., Selcen, D. and Sine, S.M. (2015) Congenital myasthenic syndromes: pathogenesis, diagnosis, and treatment. *Lancet Neurol.*, **14**, 420–434.
- Ohno, K., Otsuka, K. and Ito, M. (2016) Roles of collagen Q in MuSK antibody-positive myasthenia gravis. *Chem. Biol. Interact.*, **259**, 266–270.
- Ramdas, S. and Beeson, D. (2021) Congenital myasthenic syndromes: where do we go from here? *Neuromuscul. Disord.*, **31**, 943–954.
- Huze, C., Bauche, S., Richard, P., Chevessier, F., Goillot, E., Gaudon, K., Ben Ammar, A., Chaboud, A., Grosjean, I., Lecuyer, H.A. et al. (2009) Identification of an agrin mutation that causes congenital myasthenia and affects synapse function. *Am. J. Hum. Genet.*, **85**, 155–167.
- Ohkawara, B., Cabrera-Serrano, M., Nakata, T., Milone, M., Asai, N., Ito, K., Ito, M., Masuda, A., Ito, Y., Engel, A.G. and Ohno, K. (2014) LRP4 third beta-propeller domain mutations cause novel congenital myasthenia by compromising agrin-mediated MuSK signaling in a position-specific manner. *Hum. Mol. Genet.*, **23**, 1856–1868.
- Chevessier, F., Faraut, B., Ravel-Chapuis, A., Richard, P., Gaudon, K., Bauche, S., Prioleau, C., Herbst, R., Goillot, E., Ioos, C. et al. (2005) Towards the molecular elucidation of congenital myasthenic syndromes: identification of mutations in MuSK. *Acta Myol.*, **24**, 55–59.

7. Selcen, D., Ohkawara, B., Shen, X.M., McEvoy, K., Ohno, K. and Engel, A.G. (2015) Impaired synaptic development, maintenance, and neuromuscular transmission in LRP4-related myasthenia. *JAMA Neurol.*, **72**, 889–896.
8. Beeson, D., Higuchi, O., Palace, J., Cossins, J., Spearman, H., Maxwell, S., Newsom-Davis, J., Burke, G., Fawcett, P., Motomura, M. et al. (2006) Dok-7 mutations underlie a neuromuscular junction synaptopathy. *Science*, **313**, 1975–1978.
9. Okada, K., Inoue, A., Okada, M., Murata, Y., Kakuta, S., Jigami, T., Kubo, S., Shiraishi, H., Eguchi, K., Motomura, M. et al. (2006) The muscle protein Dok-7 is essential for neuromuscular synaptogenesis. *Science*, **312**, 1802–1805.
10. Ohno, K., Ohkawara, B. and Ito, M. (2017) Agrin-LRP4-MuSK signaling as a therapeutic target for myasthenia gravis and other neuromuscular disorders. *Expert Opin. Ther. Targets*, **21**, 949–958.
11. Rodriguez Cruz, P.M., Cossins, J., Cheung, J., Maxwell, S., Jayawant, S., Herbst, R., Waithe, D., Kornev, A.P., Palace, J. and Beeson, D. (2020) Congenital myasthenic syndrome due to mutations in MUSK suggests that the level of MuSK phosphorylation is crucial for governing synaptic structure. *Hum. Mutat.*, **41**, 619–631.
12. Inoue, A., Setoguchi, K., Matsubara, Y., Okada, K., Sato, N., Iwakura, Y., Higuchi, O. and Yamanashi, Y. (2009) Dok-7 activates the muscle receptor kinase MuSK and shapes synapse formation. *Sci. Signal.*, **2**, ra7.
13. Buyan, A., Kalli, A.C. and Sansom, M.S. (2016) Multiscale simulations suggest a mechanism for the association of the Dok7 PH domain with PIP-containing membranes. *PLoS Comput. Biol.*, **12**, e1005028.
14. Bergamin, E., Hallock, P.T., Burden, S.J. and Hubbard, S.R. (2010) The cytoplasmic adaptor protein Dok7 activates the receptor tyrosine kinase MuSK via dimerization. *Mol. Cell*, **39**, 100–109.
15. Hamuro, J., Higuchi, O., Okada, K., Ueno, M., Iemura, S., Natsume, T., Spearman, H., Beeson, D. and Yamanashi, Y. (2008) Mutations causing DOK7 congenital myasthenia ablate functional motifs in DOK-7. *J. Biol. Chem.*, **283**, 5518–5524.
16. Hallock, P.T., Xu, C.F., Park, T.J., Neubert, T.A., Curran, T. and Burden, S.J. (2010) Dok-7 regulates neuromuscular synapse formation by recruiting Crk and Crk-L. *Genes Dev.*, **24**, 2451–2461.
17. Muller, J.S., Mihaylova, V., Abicht, A. and Lochmuller, H. (2007) Congenital myasthenic syndromes: spotlight on genetic defects of neuromuscular transmission. *Expert Rev. Mol. Med.*, **9**, 1–20.
18. Selcen, D., Milone, M., Shen, X.M., Harper, C.M., Stans, A.A., Wieben, E.D. and Engel, A.G. (2008) Dok-7 myasthenia: phenotypic and molecular genetic studies in 16 patients. *Ann. Neurol.*, **64**, 71–87.
19. Liewluck, T., Selcen, D. and Engel, A.G. (2011) Beneficial effects of albuterol in congenital endplate acetylcholinesterase deficiency and Dok-7 myasthenia. *Muscle Nerve*, **44**, 789–794.
20. Witting, N. and Vissing, J. (2014) Pharmacologic treatment of downstream of tyrosine kinase 7 congenital myasthenic syndrome. *JAMA Neurol.*, **71**, 350–354.
21. Cossins, J., Liu, W.W., Belaya, K., Maxwell, S., Oldridge, M., Lester, T., Robb, S. and Beeson, D. (2012) The spectrum of mutations that underlie the neuromuscular junction synaptopathy in DOK7 congenital myasthenic syndrome. *Hum. Mol. Genet.*, **21**, 3765–3775.
22. Takeda, J.I., Nanatsue, K., Yamagishi, R., Ito, M., Haga, N., Hirata, H., Ogi, T. and Ohno, K. (2020) InMeRF: prediction of pathogenicity of missense variants by individual modeling for each amino acid substitution. *NAR Genom. Bioinform.*, **2**, lqaa038.
23. Mihaylova, V., Scola, R.H., Gervini, B., Lorenzoni, P.J., Kay, C.K., Werneck, L.C., Stucka, R., Guergueltcheva, V., von der Hagen, M., Huebner, A. et al. (2010) Molecular characterisation of congenital myasthenic syndromes in southern Brazil. *J. Neurol. Neurosurg. Psychiatry*, **81**, 973–977.
24. Miyana, K., Ishiyama, A., Saito, Y. and Nishino, I. (2022) Tulobuterol is a potential therapeutic drug in congenital myasthenic syndrome. *Pediatr. Int.*, **64**, e15115.
25. Ueta, R., Tezuka, T., Izawa, Y., Miyoshi, S., Nagatoishi, S., Tsumoto, K. and Yamanashi, Y. (2017) The carboxyl-terminal region of Dok-7 plays a key, but not essential, role in activation of muscle-specific receptor kinase MuSK and neuromuscular synapse formation. *J. Biochem.*, **161**, 269–277.
26. Johnston, H.E. and Samant, R.S. (2021) Alternative systems for misfolded protein clearance: life beyond the proteasome. *FEBS J.*, **288**, 4464–4487.
27. Frenz, B., Lewis, S.M., King, I., DiMaio, F., Park, H. and Song, Y. (2020) Prediction of protein mutational free energy: benchmark and sampling improvements increase classification accuracy. *Front. Bioeng. Biotechnol.*, **8**, 558247.
28. Strokach, A., Corbi-Verge, C. and Kim, P.M. (2019) Predicting changes in protein stability caused by mutation using sequence- and structure-based methods in a CAGIS blind challenge. *Hum. Mutat.*, **40**, 1414–1423.
29. Ben Ammar, A., Petit, F., Alexandri, N., Gaudon, K., Bauche, S., Rouche, A., Gras, D., Fournier, E., Koenig, J., Stojkovic, T. et al. (2010) Phenotype genotype analysis in 15 patients presenting a congenital myasthenic syndrome due to mutations in DOK7. *J. Neurol.*, **257**, 754–766.
30. Oury, J., Zhang, W., Leloup, N., Koide, A., Corrado, A.D., Ketavarapu, G., Hattori, T., Koide, S. and Burden, S.J. (2021) Mechanism of disease and therapeutic rescue of Dok7 congenital myasthenia. *Nature*, **595**, 404–408.
31. Koyuncu, S., Saez, I., Lee, H.J., Gutierrez-Garcia, R., Pokrzywa, W., Fatima, A., Hoppe, T. and Vilchez, D. (2018) The ubiquitin ligase UBR5 suppresses proteostasis collapse in pluripotent stem cells from Huntington's disease patients. *Nat. Commun.*, **9**, 2886.
32. Noormohammadi, A., Khodakarami, A., Gutierrez-Garcia, R., Lee, H.J., Koyuncu, S., Konig, T., Schindler, C., Saez, I., Fatima, A., Dieterich, C. et al. (2016) Somatic increase of CCT8 mimics proteostasis of human pluripotent stem cells and extends *C. elegans* lifespan. *Nat. Commun.*, **7**, 13649.
33. Vilchez, D., Boyer, L., Morantte, I., Lutz, M., Merkwirth, C., Joyce, D., Spencer, B., Page, L., Masliah, E., Berggren, W.T., Gage, F.H. and Dillin, A. (2012) Increased proteasome activity in human embryonic stem cells is regulated by PSMD11. *Nature*, **489**, 304–308.
34. Iberite, F., Gruppioni, E. and Ricotti, L. (2022) Skeletal muscle differentiation of human iPSCs meets bioengineering strategies: perspectives and challenges. *NPJ Regen. Med.*, **7**, 23.
35. Pettit, R.S. and Fellner, C. (2014) CFTR modulators for the treatment of cystic fibrosis. *P T*, **39**, 500–511.
36. Lukacs, G.L. and Verkman, A.S. (2012) CFTR: folding, misfolding and correcting the DeltaF508 conformational defect. *Trends Mol. Med.*, **18**, 81–91.
37. Fiedorczyk, K. and Chen, J. (2022) Mechanism of CFTR correction by type I folding correctors. *Cell*, **185**, 158–168 e111, 158, 168.e11.
38. Tran, M.L., Genisson, Y., Ballereau, S. and Dehoux, C. (2020) Second-generation pharmacological chaperones: beyond inhibitors. *Molecules*, **25**, 3145.

39. Okita, K., Matsumura, Y., Sato, Y., Okada, A., Morizane, A., Okamoto, S., Hong, H., Nakagawa, M., Tanabe, K., Tezuka, K. et al. (2011) A more efficient method to generate integration-free human iPS cells. *Nat. Methods*, **8**, 409–412.
40. Okita, K., Yamakawa, T., Matsumura, Y., Sato, Y., Amano, N., Watanabe, A., Goshima, N. and Yamanaka, S. (2013) An efficient nonviral method to generate integration-free human-induced pluripotent stem cells from cord blood and peripheral blood cells. *Stem Cells*, **31**, 458–466.
41. Takahashi, K., Tanabe, K., Ohnuki, M., Narita, M., Ichisaka, T., Tomoda, K. and Yamanaka, S. (2007) Induction of pluripotent stem cells from adult human fibroblasts by defined factors. *Cell*, **131**, 861–872.
42. Uchimura, T., Otomo, J., Sato, M. and Sakurai, H. (2017) A human iPS cell myogenic differentiation system permitting high-throughput drug screening. *Stem Cell Res.*, **25**, 98–106.
43. Maurissen, T.L. and Woltjen, K. (2020) Synergistic gene editing in human iPS cells via cell cycle and DNA repair modulation. *Nat. Commun.*, **11**, 2876.
44. Arslan, M.A., Chikina, M., Csermely, P. and Soti, C. (2012) Misfolded proteins inhibit proliferation and promote stress-induced death in SV40-transformed mammalian cells. *FASEB J.*, **26**, 766–777.